Hemodynamic Variables Analysis in Basilar Tip Aneurysms with a Novel Bypass Approach: A CFD Simulation

Nusrat Tamanna Mim[1], Sorowar Hossain[2], Muhammad Sajjad Hossain[1,*]

[1]*Department of Arts and Sciences, Ahsanullah University of Science and Technology, Dhaka 1208, Bangladesh*
[2]*Department of Applied Mathematics, University of Dhaka, Dhaka 1000, Bangladesh*

***Corresponding author.**

Abstract.*Cerebral artery disease is a leading global cause of mortality. Bypass graft surgery, a therapeutic intervention aimed at restoring blood circulation, represents an effective approach for the treatment of this ailment. The present work conducted an analysis and developed an idealized, 3D cerebral aneurysm model with a novel complete bypass graft to treat the aneurysm. Several bypass cases were considered according to Table 1 to determine the optimal combination by analyzing the hemodynamic parameters, i.e., blood pressure, velocity, and wall shear stress (WSS). The Finite Volume Method (FVM) was used for numerical simulations. The results showed that at the peak of the systolic phase, averaged pressure and averaged WSS fell to about 27–38% and 35–57%, respectively, at the aneurysm wall, while the velocity dropped to about 23–45% inside the aneurysm. By analyzing numerical results, case 4 was found to be optimal. In this case, for the peak of the systolic phase, averaged pressure and averaged WSS reduced to ~37.979% and ~56.662%, respectively, for the aneurysm wall, and averaged velocity reduced to ~44.934% inside the aneurysm. These findings could serve as a reference for medical intervention as well.*

Keywords: Pulsatile blood flow, Cerebral artery, Aneurysm, Bypass graft, Finite volume method.

1. INTRODUCTION

Cerebral aneurysms (CAs) commonly known as intracranial or brain aneurysms, which can affect 3% to 5% of the worldwide population, are abnormal dilations of cerebral blood arteries that present considerable dangers to neurological health and general survival[1, 2]. Aneurysms develop from weak artery walls, usually around bifurcation sites, and may stay symptomless until rupture, resulting in severe outcomes such as aneurysmal subarachnoid hemorrhage (aSAH), a critical condition linked to higher morbidity and mortality rates[2, 3].The reported rate of aSAH due to a burst intracranial aneurysm in the United States is roughly 8-10 per 100,000 individuals, with nearly 500,000 fatalities globally each year attributed to brain aneurysms[4].Behavioral risks for aneurysmal subarachnoid hemorrhage (aSAH) encompass hypertension, tobacco usage, alcohol dependence, and the consumption of sympathomimetic substances like cocaine, while women are more predisposed than men to develop a brain aneurysm, with a ratio of 3:2[4, 5].Therefore, to lower the mortality rate, it is essential to have a solid understanding of the flow characteristics of brain aneurysm.Computer simulations or numerical analyses offer researchers efficient methods to comprehend the flow characteristics or hemodynamics such as blood pressure, Wall Shear Stress (WSS), and blood velocity of aneurysms, facilitating the detection of aneurysms and their critical conditions, as well as aiding in their treatment[6-10]. Despite the elastic nature of the walls of the arteries and aneurysms, they are treated as rigid and sometimes idealized modelsare considered in the place of patient specific models in order to facilitate numerical simulation of the models. So, Zhao et al. [11]conducted numerical simulations of the aneurysm model and presented a comparative analysis of the results, treating arterial and aneurysmal walls as rigid and elastic, respectively. They demonstrated that elastic models align remarkably well with the clinical environment[11].Ford et al.[8] conducted a numerical study demonstrating that computational fluid dynamics (CFD) is capable of accurately modeling the intra-aneurysmal flow characteristics in structurally realistic experimental models. In other study,Bernsdorf et al. [12]examined the disparity in WSS between Newtonian and non-Newtonian fluids in a patient-specific cerebral aneurysm model, demonstrating that the maximal Newtonian WSS is 17-50% more than that observed in the non-Newtonian simulation.Furthermore, several studies have been done to analyze the risk factors, and it is found that WSS, pressure, oscillatory shear index (OSI), etc. are key factors in developing an aneurysm[13-20]. In a study, Kaneko et al.[21] demonstrated that, using an in vitro model of cerebral aneurysm, that the basilar tip aneurysm's peak experiences low WSS and circulating flow, while the parent artery has linear flow. Similarly, Jiang et al.[22]and Singh et al. [19]demonstrated that hemodynamic characteristics linked with thinner aneurysm wall sections included higher pressure and lower WSS and there are considerable risk of rupture. Various investigations by Kimura et al.[16] and Qi Hu et al. [23]demonstrated that maximum OSI is a critical determinant of rupture risk, while low OSI is significantly associated with the thin-walled regions of cerebral aneurysms.Fujimura et al.[17] examined the hemodynamic factors associated with aneurysm beginning by analyzing angiographic images of patients with cerebral aneurysms obtained prior to and following aneurysm formation. They concluded that beginning of aneurysm is more probable in regions where both tensile forces exerted on theartery wall and total pressure loss are substantial[17]. Moreover, the above researchers didn’t show the treatment plan for cerebral aneurysms.Various surgical treatments exist for the treatment of cerebral aneurysms, including clipping, wrapping and clipping, coil embolization, high-porosity mesh (HPM) stents, and bypass procedures [24-31]. Also, a novel technique known as a flow diverter stent has been proposed for the treatment of aneurysms[32, 33].In a study, Feng et al.[34] demonstrated that the clip-on-wrapping method can be used to fix an aneurysm neck avulsion where the cracked area can't be closed. Although clipping is an effective option for ruptured aneurysms, nevertheless, it is subject to specific limitations about the aneurysm's location, size, and shape [25, 35].

In the treatment of an intracranial aneurysm, the coiling procedure is considered to be a major and customary alternative. But Coil displacement represents a significant complication associated with embolization procedures. It may lead to infarcts associated with asymptomatic strokes in less severe instances, whereas in severe cases, it could obstruct major branches, leading to extensive territory damage [24].To implement the stent method,Qiu et al.[25]demonstrated that the use of an HPM stent can reduce the velocity, pressure, wall shear stress, and energy loss of blood flow within the aneurysm by 30-40%. However, complications such as stent displacement and migration, thrombosis, vascular damage, and in-stent restenosis may render its use inappropriate[24].Moreover, a flow diverter stent is unsuitable for bifurcation aneurysms, such as basilar tip aneurysms, due to the potential for ischemia problems or thrombosis in the obstructed side branches associated with flow-diverting procedures[33].Under these conditions, bypass techniques such as extracranial-intracranial (EC-IC) or intracranial-intracranial (IC-IC) are used to fix basilar tip aneurysms[24, 26, 35, 36].In a study using a model of an idealized basilar tip aneurysm, Kurşun et al. [26] examined flow velocity, pressure, and wall shear stress (WSS), demonstrating that pressure and WSS can be lowered by 40-70% at the aneurysm wall using a bypass approach. However, their model lacked key arteries, such as the superior cerebral arteries. They also used a patient-specific velocity profile from Qiu et al.[25], but they failed to integrate it into their velocity profile equation. The present study addressed and resolved these issues.

This work used a computational fluid dynamics (CFD) system to assess the influence of the bypass graft on a simplified model of a basilar tip aneurysm. The novelty of this work lies in its ability to bypass both the superior cerebral arteries and the posterior cerebral arteries, which originate from the basilar artery, while treating blood as pulsatile and non-Newtonian.The finite volume method (FVM) was employed for numerical computation, and the Carreau-Yasuda model was utilized for non-Newtonian blood viscosity. The impact of bypass graft configurations is analyzed regarding hemodynamic parameters, including velocity, pressure, and wall shear stress (WSS). This is due to the fact that these parameters are crucial in the formation, progression, and eventual rupture of aneurysms. This research aimed to ascertain the appropriate bypass conditions by examining the hemodynamic indices inside the model and assessing their variations based on the positioning of the bypass connection and the diameter of the bypass arteries. Also, a comparison between Newtonian and non-Newtonian fluids was conducted.

2. MATHEMATICAL FORMULATION

2.1 Physical model

Figure 1 shows the geometrical model of the desired simulation. Several models were considered to simulate a simplified cerebral aneurysm condition with complete bypass treatment. These idealized models were simplified from the patient-specific model studied by Appanaboyina et al. [37], which is shown in Figure 1(c). For these studies, a spherical aneurysm with a diameter of D=8 mm was placed on the junction of the right posterior cerebral artery (RPCA), the left posterior cerebral artery (LPCA), and the basilar artery (BA). Figure 1(a) depicts the model prior of bypass surgery consisting of RPCA, LPCA, BA, right superior cerebral artery (RSCA), and left superior cerebral artery (LSCA).

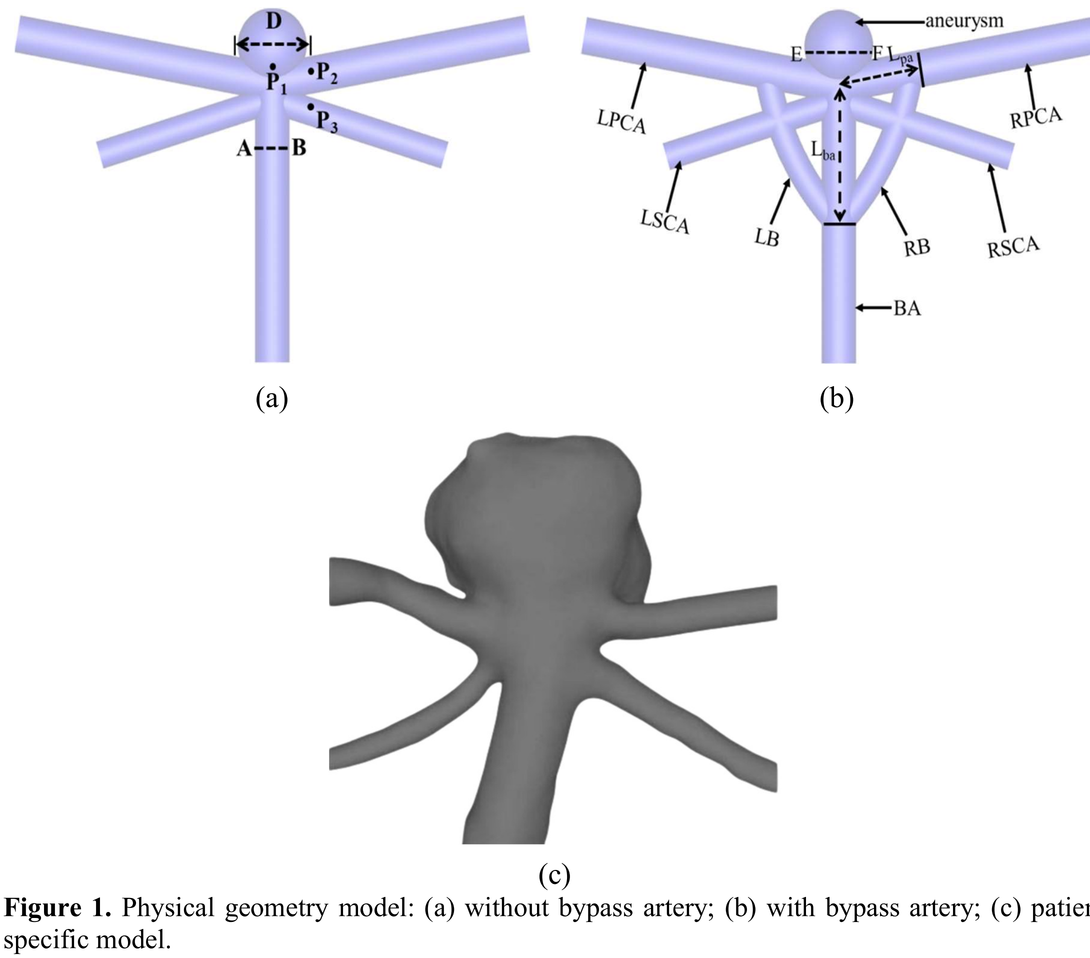

Figure 1. Physical geometry model: (a) without bypass artery; (b) with bypass artery; (c) patient specific model.

Also, Figure 1(b) shows the model with a complete bypass graft. For this model, the diameters of RPCA, LPCA, and BA is 4mm and the diameters of RSCA and LSCA is 3mm were taken. Furthermore, the RPCA, LPCA, and BA lengths are 30 mm; on the other hand, the lengths of RSCA and LSCA were considered 20 mm. For the bypass cases, the anastomotic angle was chosen at nearly 45°. To analyze the flow phenomena, two pathways was considered with namely, AB: $-2\,mm \le x \le 2\,mm,\ y=-6\,mm,\ z=0\,mm$, andEF: $-4\,mm \le x \le 4\,mm,\ y=4\,mm,\ z=0\,mm$, and several points were chosen on the coronal plane which are: P_1(0, 3.5, 0) placed on aneurysm, P_2(5, 1.5, 0) placed on PCA, P_3(5, -3, 0) placed on SCA. Furthermore, several simulations were conducted for various diameters of the bypass arteries (RB: right bypass, LB: left bypass) and several locations were chosen on RPCA, LPCA, RSCA, LSCA, and BA to perform the surgery, which is given in Table 1.

Table 1: The different values of different cases that are considered during numerical study

Cases	Length on BA, L_{ba}(mm)	Length on PCA, L_{pa}(mm)	Diameter of bypass arteries, d (mm)
Case 1	15	10	2.5
Case 2	20	16	2.5
Case 3	15	10	3
Case 4	20	16	3

2.2 Governing equations

The continuity and the momentum (Navier-Stokes) equations that represents the laminar blood flow in a cerebral artery with a bypass graft written as follows:

Continuity equation:

$$\frac{\partial \rho}{\partial t} + \vec{\nabla} \cdot (\rho \vec{V}) = 0 \tag{1}$$

Momentum equation:

$$\rho\left(\frac{\partial \vec{V}}{\partial t} + \vec{V} \cdot \vec{\nabla}\vec{V}\right) = -\vec{\nabla}P + \eta\,\vec{\nabla}^2\vec{V} + \rho\vec{g} \tag{2}$$

Where ρ is the blood density, $\vec{V}$ is the velocity vector, t is the time, p is the pressure and for the $\eta$is the fluid viscosity.For the non-Newtonian blood flow, the viscosity of fluid is dependent onthe shear rate ($\dot{\gamma}$) andCarreau-Yasuda model was used for these studies and the viscosity, ηdefined as follows:

$$\eta(\dot{\gamma}) = \eta_0 + (\eta_0 - \eta_\infty)\left[1 + \lambda(\dot{\gamma})^{\alpha}\right]^{\left(\frac{n-1}{\alpha}\right)} \tag{3}$$

Here, the zero shear viscosity, $\eta_0 = 0.16\,Pa.s$, the infinite shear viscosity, $\eta_\infty = 0.0035\,Pa.s$, the characteristic relaxation time, $\lambda = 8.2\,s$, power law index, $n = 0.2128$, and the Yasuda exponent, $\alpha = 1.23$.

2.3 Initial and Boundary conditions

For these numerical studies, the blood flow considered as laminar and incompressible with density $\rho = 1060\ kg/m^3$ and dynamic viscosity, $\eta = 0.0035\ Pa.s$ was used for a Newtonian blood flow.

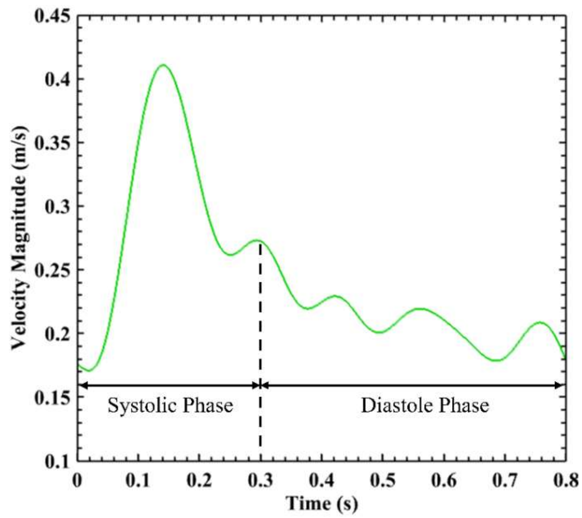

Figure 2: Theinlet velocity profile.

For non-Newtonian blood flow, Carreau-Yasuda model was used taken from the previous study [38] and defined in equation (3). In the inlet of the geometrises, the pulse inlet velocity condition with heart rate 75 beats per minute was used which is the time dependent function. A single cycle was used for the numerical simulation taken from the previous study[25, 26]. In Figure 2, the inlet velocity is shown, and equation (4) described the inlet velocity which is defined as the summation of sine functions.
The inlet velocity equation is:

$$v(t) = \sum_{i=1}^{7} a_i \sin(b_i t + c_i) \tag{4}$$

a_i, b_i, and c_i are the parameters of this equation and values of these parametersare given in Table 2.

Table 2.values of the parameters of inlet velocity.

a_i	b_i	c_i
0.2812	2.5275	0.8069
0.0770	11.5965	-0.4339
0.0403	17.3407	-0.2073
0.0218	29.4373	-2.8273
0.0323	38.1356	-4.5358
0.0317	40.3051	3.4551
0.0052	55.1373	3.4653

The velocity of the arteries wall, $v(t) = 0$ and initially the gauge pressure of the outletwas set to zero.

3. NUMERICAL PROCEDURE WITH VALIDATION AND GRID TEST

The continuity, momentum and associated boundary conditions were numerically simulated using the Finite Volume Method (FVM) in this study,. To describe the blood flow phenomenon within the model, all computational methods were implemented utilizing Ansys Fluent software. The SIMPLE scheme method was used for pressure-velocity coupling. On the other hand, the Second-Order spatial discretization method was used for pressure, and the Second Order Upwind was used for Momentum.

After the grid independence test which is shown in Figure 3(c-d), an unstructured tetrahedral grid was used in the geometrical domain. In the bifurcation area, grid sizes of 0.1 mm and 0.2 mm were set in the otherdomain area.Number of elements was chosen nearly 900k. For the solution, a time step size of 0.0001 s was used during calculations. The convergence tolerance was set at 1×10^{-3} to assure the accuracy of the solutions, and equation (5) was used to ensure the criteria.

$$\left|\frac{\zeta_{m+1}(p,q,r)-\zeta_{m}(p,q,r)}{\zeta_{m+1}(p,q,r)}\right|\leq 1\times10^{-3} \tag{5}$$

Where ζ is any variable, m+1, and m are two consecutive iterations, and*p, q, r*are the grid locations at the directions of x, y, and z axes respectively.

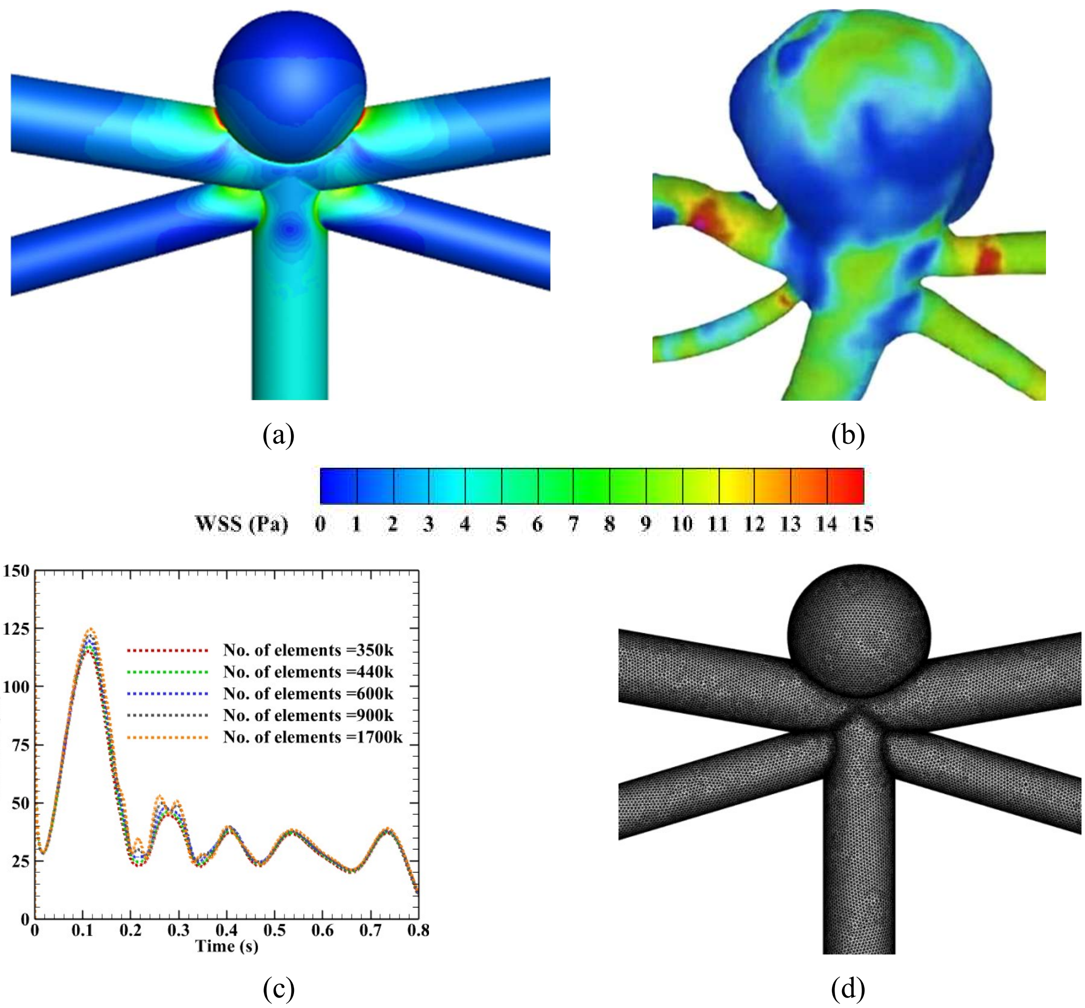

Figure 3. Comparison: Wall Shear Stress (WSS) at the peak of the systolic phase. (a) present results and (b) former patient specific study.Grid independence test: (c) pressure profiles for different number of elements at aneurysm wall; (d) structure of mesh.

Figure 3(a-b) illustrates the comparison of WSS distribution between the current study and the prior research conducted by Appanaboyina et al.[37].The distribution of WSS exhibits the same pattern in both investigations, with larger values observed in close proximity to the aneurysm. Due to structural differences between the idealized model and the actual basilar tip aneurysm, the two sets of data are not identical. After careful consideration, it was determined that the patient-specific model and the idealized model that had been developed for numerical analysis were in agreement.

4. RESULTS

The impact of the hemodynamic parameters on comparison of Newtonian and Non-Newtonian blood flow, different hemodynamic factors, pressure, velocity profiles and wall shear stress (WSS) at the peak of the systolic and diastolic phase have been discussed graphically in the figs. 4 – 12. The findings of this research work demonstrate variations in flow phenomena during cerebral aneurysms at the basilar tip, both with and without bypass surgery. The analysis follows below:

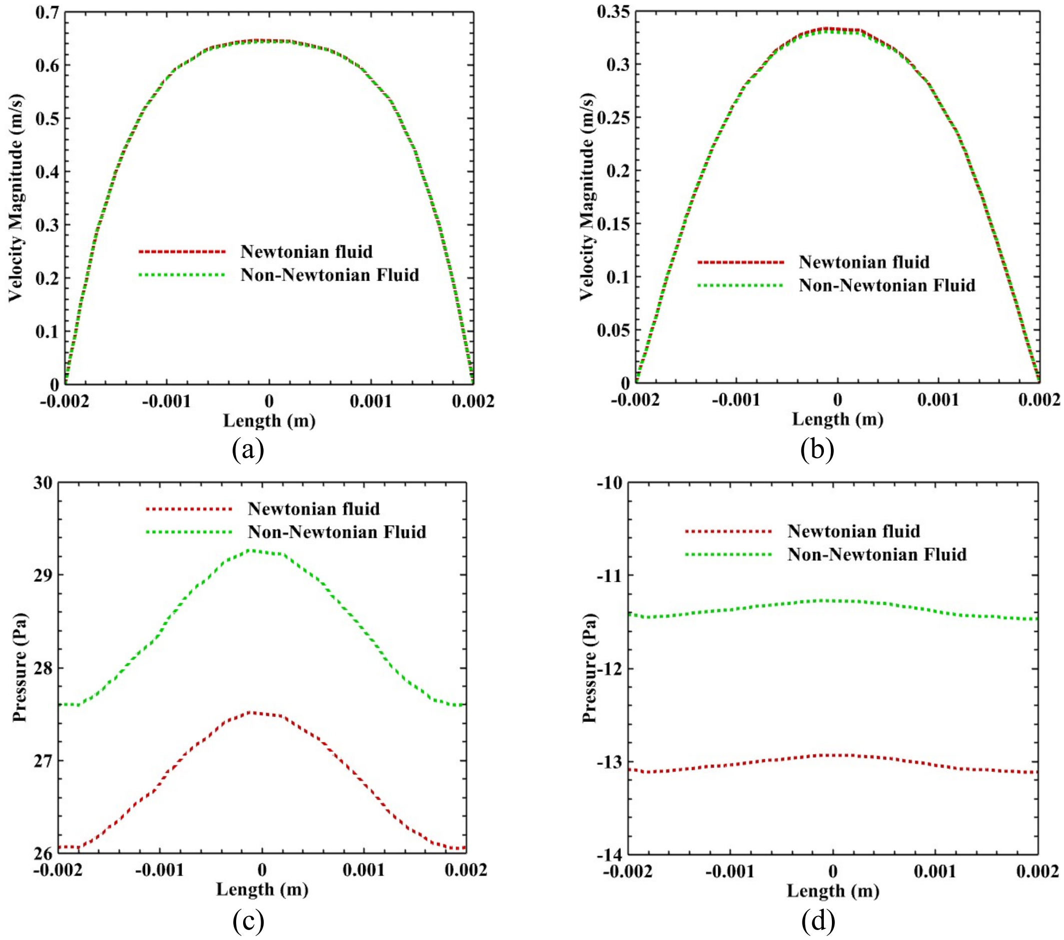

Figure 4.comparison of Newtonian and Non-Newtonian blood flow for several cases at line AB before the bypass.

Figure 4(a) illustrates the variations in velocity along line AB, accounting for blood viscosity as both Newtonian and non-Newtonian at the peak of the systolic phase (0.145 s). Conversely, Figure 4(b) depicts the velocity alterations at the end of the diastolic phase (0.8 s), also considering blood as Newtonian and non-Newtonian. Likewise, Figure 4(c) illustrates the pressure profile at the highest point of the systolic phase, whereas Figure 4(d) depicts the pressure at the end of the diastolic period. In scenario 4(a), the maximum velocity for the Newtonian fluid is 0.64592 m/s, whereas for the non-Newtonian fluid, it is 0.643825 m/s. Additionally, in scenario 4(b), the velocity of non-Newtonian blood flow decreases to 0.953% of the maximum Newtonian blood flow (0.334 m/s).In case 4(c), non-Newtonian blood pressure increased around ~6.356% relative to Newtonian blood pressure, but in case 4(d), the increase was approximately 12.859%.

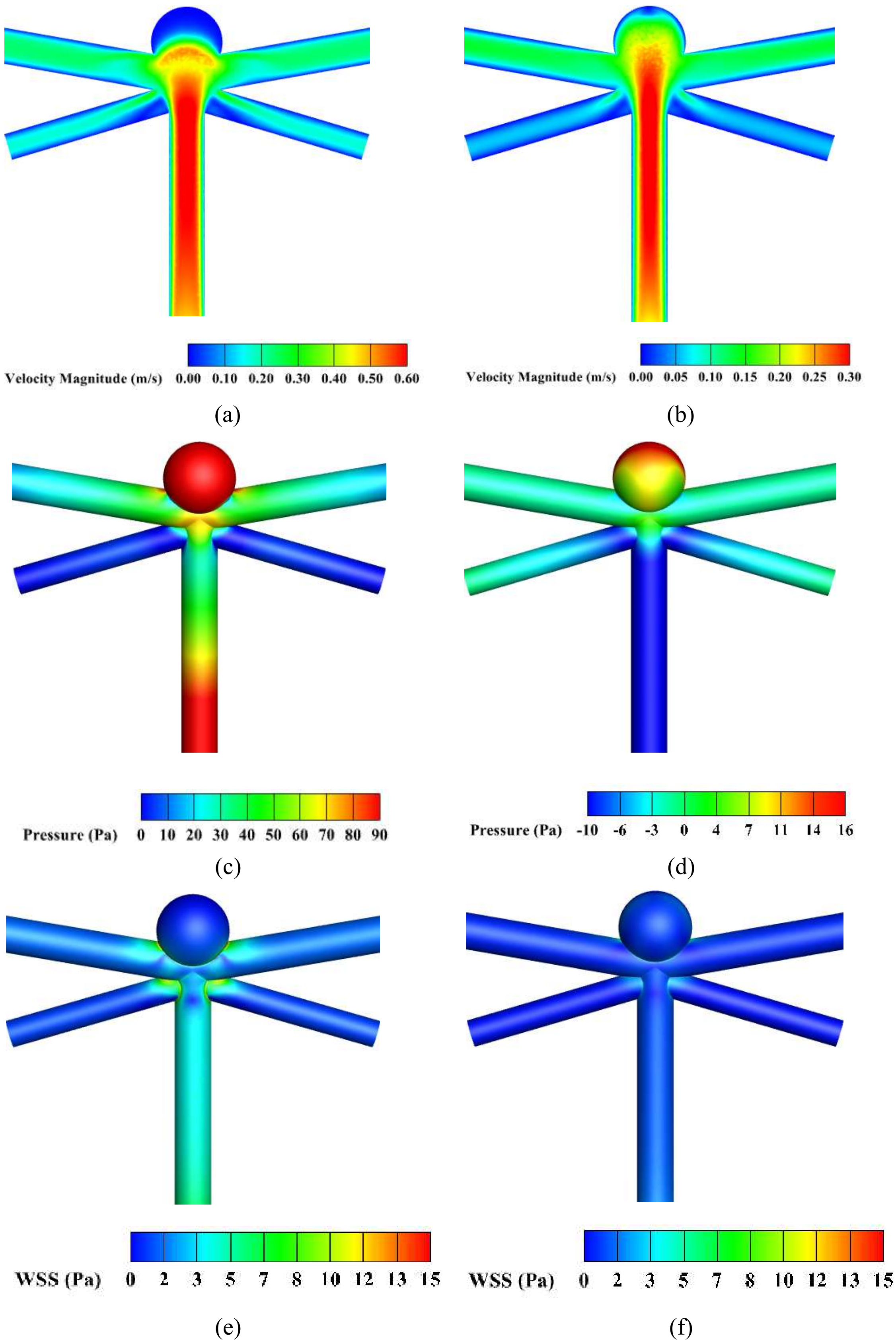

Figure 5. View of different hemodynamic factors into the model before the bypass surgery.

There are several hemodynamic parameters that are depicted in Figure 5. These include 5(a) the magnitude of the velocity on the coronal plane, 5(c) the pressure, and 5(e) the wall shear stress profiles on the artery walls during the peak time of the systolic phase (0.145s). On the other hand, the profiles of velocity, pressure, and wall shear stress at the conclusion of the diastolic phase (0.8s) are described by equations 5(b), 5(d), and 5(f). It has been discovered that the vast majority of the velocity magnitude distribution is located in the middle of the basilar artery, as shown in Figures 5(a-b). According to figure 5(a), the velocity at positionsP_1, P_2, and$P_3$are approximately 0.466 m/s, 0.271 m/s, and 0.172 m/s, respectively. Additionally, the mass flow rate at the PCA exit is around 2.107 g/s, while at the SCA outlet, it is approximately 0.7105 g/s. In the case of 5(b), it has been determined that the velocities at positionsP_1, P_2, and$P_3$are approximately 0.234 m/s, 0.125 m/s, and 0.081 m/s, respectively. The mass flow rate at the PCA outlet is around 0.969 g/s, while at the SCA outlet, it is approximately 0.214 g/s.InFigure 5(c), the maximum pressure at the aneurysm wall is ~135.98 Pa, at the PCA wall is ~89.93 Pa, and at the SCA wall is ~56.02 Pa. In section 5(d), the maximum pressures at the aneurysm walls, PCA, and SCA are approximately 22.59 Pa, 12.45 Pa, and 0.21 Pa, respectively. In scenario 5(e), the maximal Wall Shear Stress (WSS) along the walls of the aneurysm, PCA, and SCA are approximately 19.11 Pa, 20.33 Pa, and 14.91 Pa, respectively. The maximal wall shear stress (WSS) at the walls of the aneurysm, PCA, and SCA are~5.96 Pa, ~8.31 Pa, and ~5.85 Pa, respectively, for the case of 5(f).

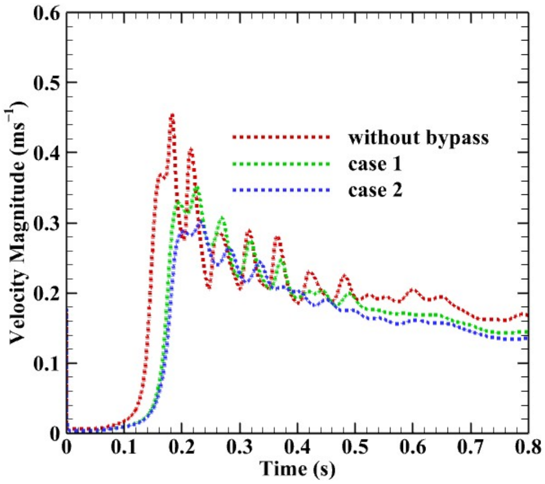

(a)

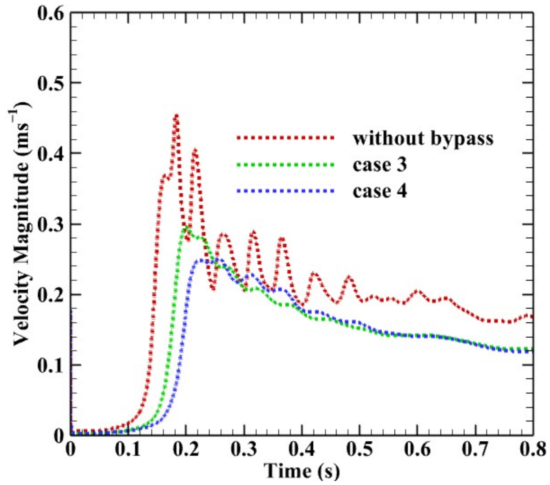

(b)

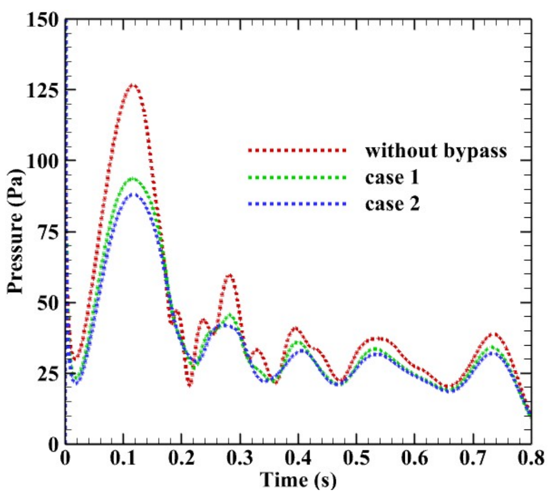

(c)

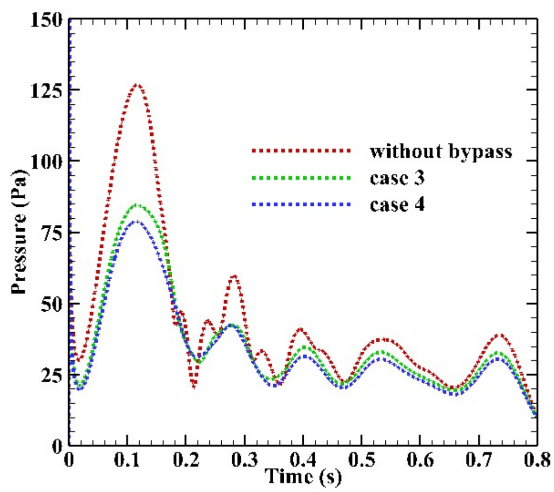

(d)

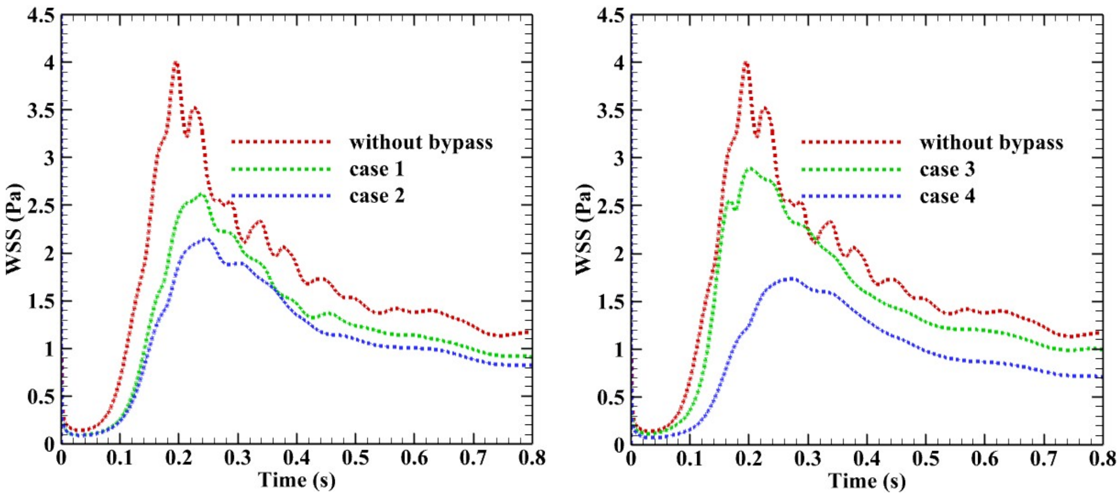

(e) (f)

Figure 6. Comparison of hemodynamic parameters for several situations with and without bypass during a cardiac cycle: (a-b) velocity along line EF; (c-d) pressure at the aneurysmal wall; (e-f) wall shear stress (WSS) at the aneurysmal wall.

Figure6(a-b) illustrates the comparison of averaged velocity along line EF for various bypass cases outlined in Table 1, as well as prior to the bypass during a cardiac cycle. In cases 1 to 4, the maximum average velocity was reduced by roughly 22.467%, 33.701%, 34.802%, and 44.934%, respectively, in comparison to the scenario without a bypass. Figure 6(c-d) similarly illustrates the contrast of average pressure at the aneurysm wall. In cases 1 to 4, the highest average pressure was reduced to roughly 26.139%, 30.448%, 33.332%, and 37.979%, respectively, in comparison to the scenario without a bypass. Figure 6(e-f) presents a comparison of the average wall shear stress (WSS) at the aneurysm wall. The results indicate that, in comparison to the scenario without bypass, the maximum average wall shear stress decreased by approximately 35.179%, 46.457%, 27.869%, and 56.662% for cases 1 through 4, respectively.

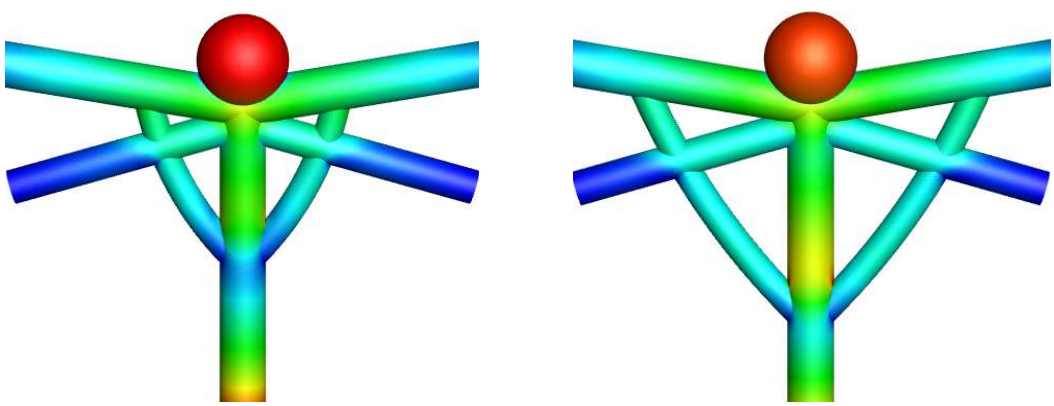

(a) (b)

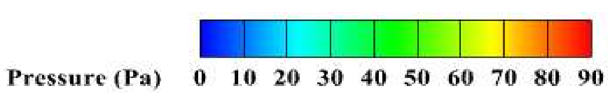

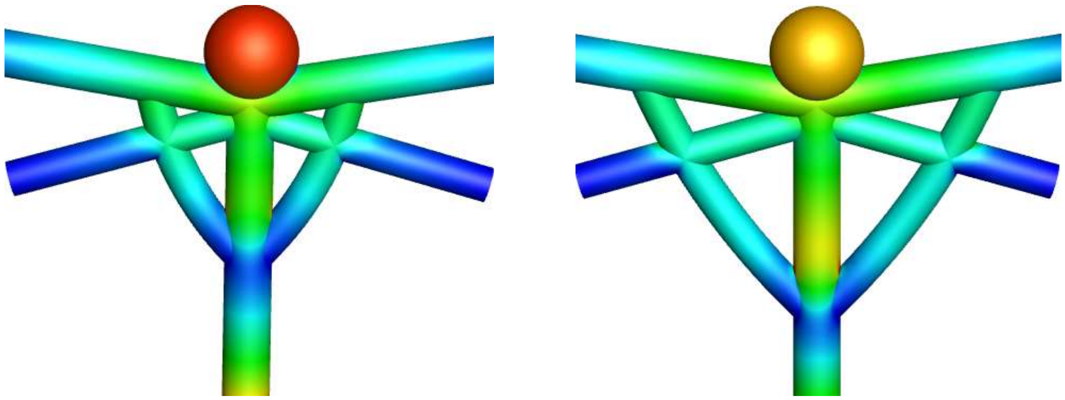

(c) (d)

Figure 7. Contours of pressure profiles at the peak of the systolic phase (0.145 s) for case 1 to case 4, as defined in Table 1.

Figure 7(a-d) depicts the artery wall's pressure at the apex of the systolic phase across several geometrical models. Figures7(a) and 7(b) correspond to cases 1 and 2, featuring a bypass artery diameter of 2.5 mm with lengths $L_{ba}$of 15 mm and 20 mm, respectively; Figures 7(c) and 7(d) represent cases 3 and 4, with a bypass artery diameter of 3 mm and lengths $L_{ba}$of 15 mm and 20 mm, respectively. From these cases, it reveals that higher pressures are distributed on the aneurysm wall.In cases 1 to 4, the maximum pressures at the aneurysm wall diminished to approximately 31.92%, 37.37%, 36.76%, and 45.96% relative to the without-bypass model. Correspondingly, at the PCA artery wall, the peak pressures reduced by approximately 29.61%, 31.88%, 32.66%, and 33.70%, respectively. Additionally, at the SCA wall, peak pressure reduced by nearly 12.82%, 14.55%, 14.08%, and 14.33% for cases 1 to 4, respectively.

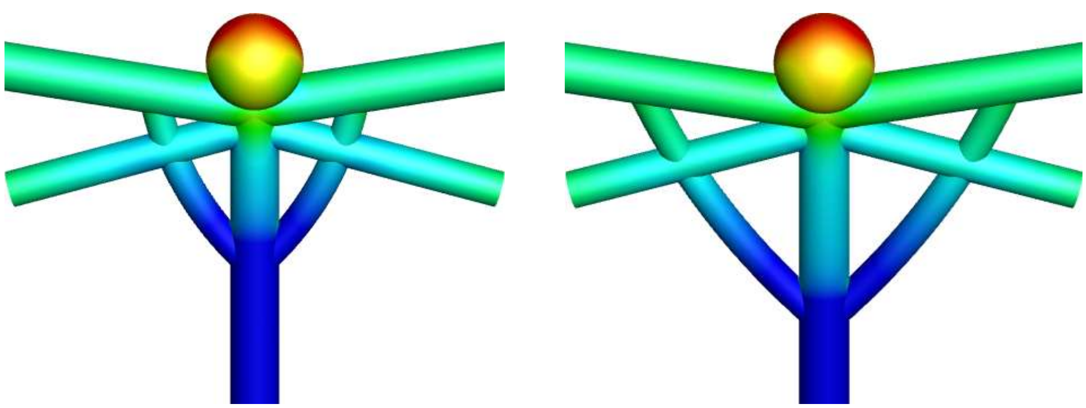

(a) (b)

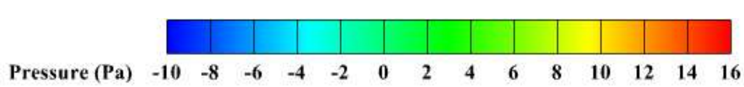

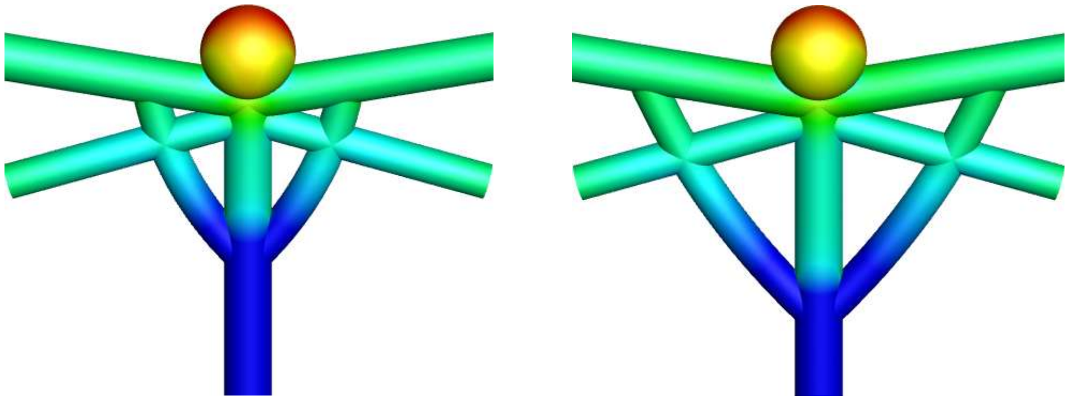

(c) (d)

Figure 8. Pressure profile contours at the end of the diastolic phase (0.8 s) for cases 1 through 4, as delineated in Table 1.

Figure 8(a-d) illustrates the arterial wall's pressure at the end of the diastolic period across several geometrical models. Figures 8(a) and 8(b) depict cases 1 and 2, whereas Figures 8(c) and 8(d) illustrate cases 3 and 4. In cases 1 to 4, peak pressures at the aneurysm wall diminished to approximately 19.79%, 23.15%, 15.89%, and 30.77%, respectively, in comparison to the model without bypass. Correspondingly, at the wall of PCA arteries, the pressure diminished by approximately 39.04%, 43.45%, 46.18%, and 48.35%, respectively. Furthermore, at the SCA wall, the maximum pressure escalated to approximately 0.48 Pa, 1.32 Pa, 1.62 Pa, and 1.89 Pa for cases 1 through 4, respectively.

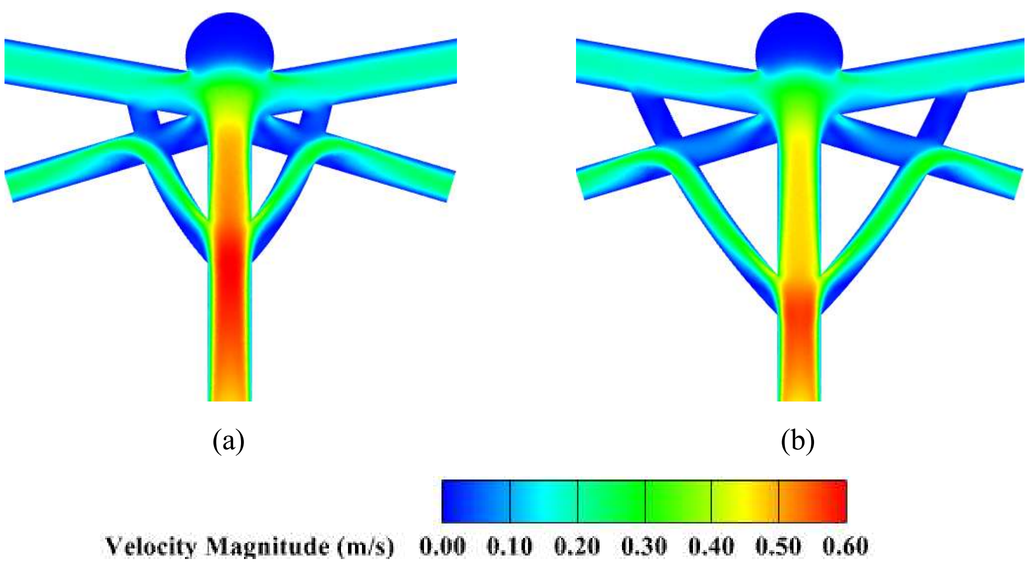

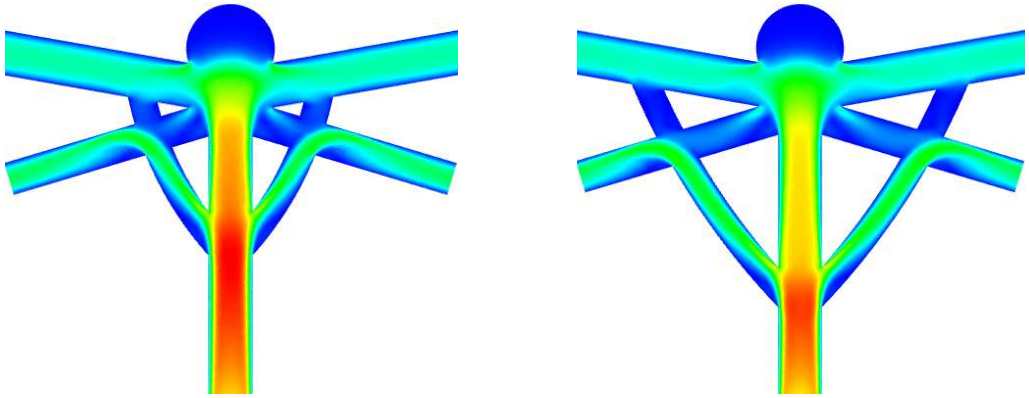

(c) (d)

Figure 9. Illustrations of velocity profiles in the coronal plane for cases 1 to 4 at the apex/peak of the systolic phase (0.145 s), respectively.

Figure 9(a-d) demonstrates the velocity in the coronal plane at the peak of the systolic phase across various geometric models. Figures 9(a) and 9(b) represent cases 1 and 2, whereas Figures 9(c) and 9(d) exemplify cases 3 and 4, as delineated in Table 1.From the contours of these scenarios, it is seen that the velocity significantly reduced in the aneurysm and the regions of PCA and SCA that are adjacent to the aneurysm due to the bypass graft. In scenarios/cases 1 to 4, the velocity at point P_1 decreased to roughly 80.78%, 85.85%, 86.02%, and 92.91%, respectively, relative to the model without bypass. At point P_2, the velocity decreased by roughly 14.31%, 22.04%, 17.27%, and 33.69%, respectively.Additionally, at point P_3, the velocity decreased by approximately 55.91%, 40.65%, 62.20%, and 33.69% for scenarios 1 through 4, respectively. The mass flow rate at the PCA outlet decreased by ~14.89%, ~32.36%, ~16.28%, and ~20.11% for the relevant cases relative to the without-bypass model. Conversely, at the SCA outlet, the mass flow rate expanded by ~42.35%, ~91.88%, ~86.29%, and ~57.13% for the corresponding scenarios analyzed in this study.

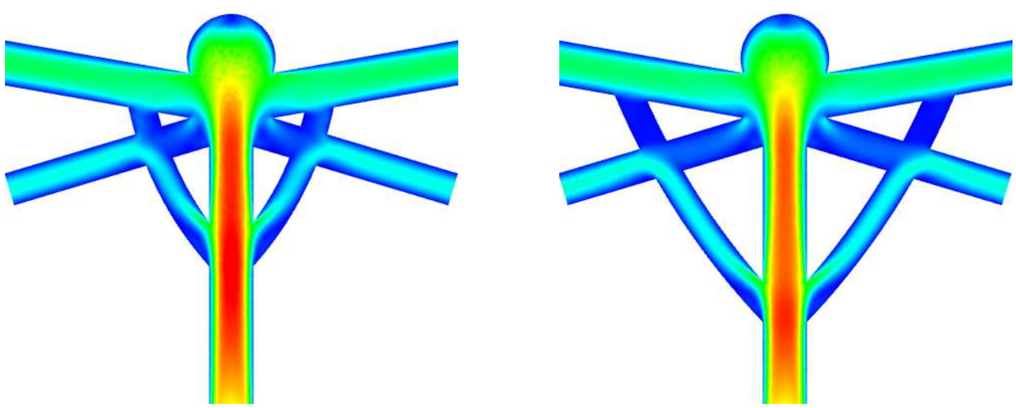

(a) (b)

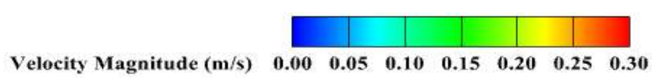

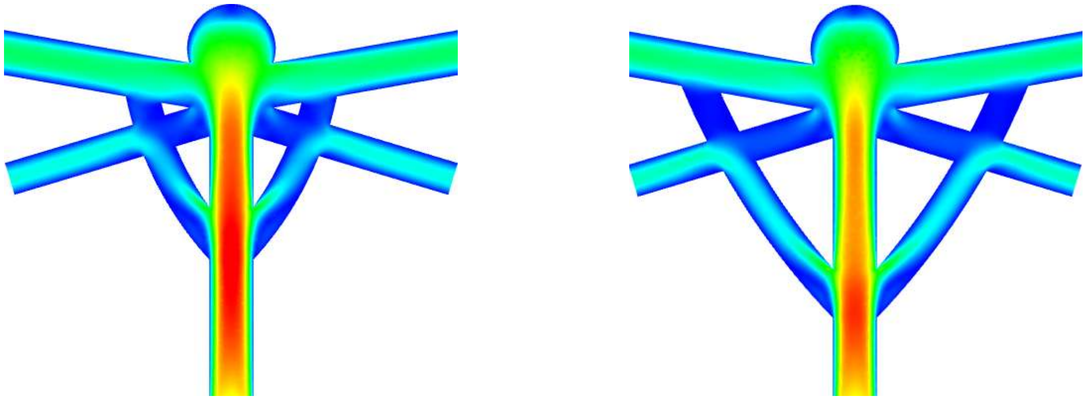

(c) (d)

Figure 10. Illustrations of velocity profiles in the coronal plane for cases 1 to 4 at the end of the diastolic phase (0.8 s), respectively.

Figure 10(a-d) illustrates the velocity in the coronal plane at the conclusion/end of the diastolic phase across several geometric models. Figures 10(a) and 10(b) illustrate cases 1 and 2, whereas Figures 10(c) and 10(d) depict cases 3 and 4, as specified in Table 1. The analysis of these scenarios reveals a substantial reduction in velocity within the aneurysm and the neighboring regions of the PCA and SCA as a result of the bypass graft. In scenarios 1 to 4, the velocity at point P_1 diminished to approximately 13.86%, 21.01%, 26.19%, and 25.50%, respectively, compared to the model without bypass. At point P_2, the velocity diminished by approximately 5.83%, 11.26%, 7.74%, and 15.97%, respectively. Furthermore, at point P_3, the velocity diminished by roughly 66.71%, 53.04%, 76.52%, and 64.59% for scenarios 1 through 4 respectively. The mass flow rate at the PCA outlet diminished by approximately 9.66%, 10.99%, 10.89%, and 13.78% for the pertinent cases compared to the model without bypass. In contrast, at the SCA outlet, the mass flow rate increased by approximately 45.05%, 52.65%, 50.76%, and 65.20% for the respective scenarios examined in this study.

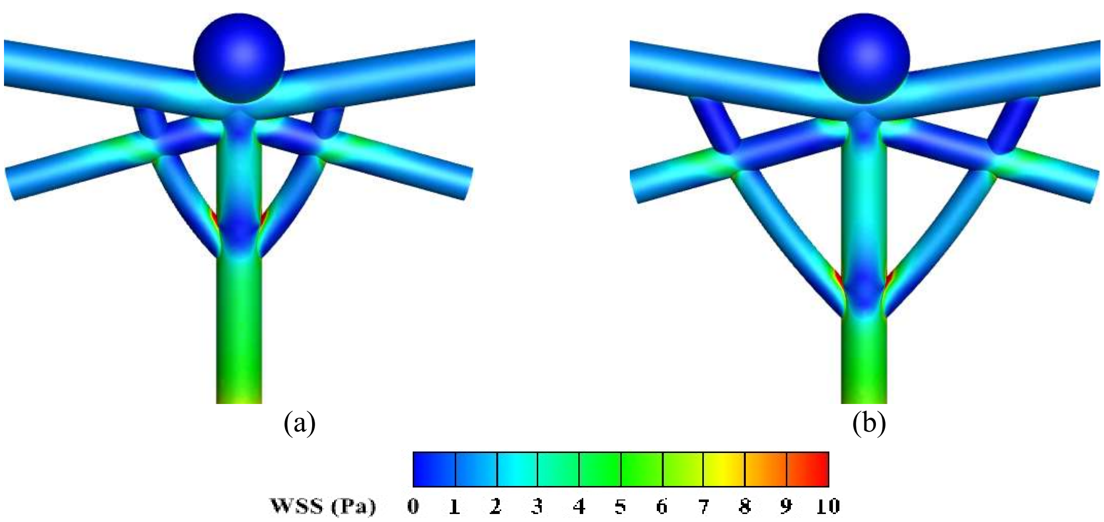

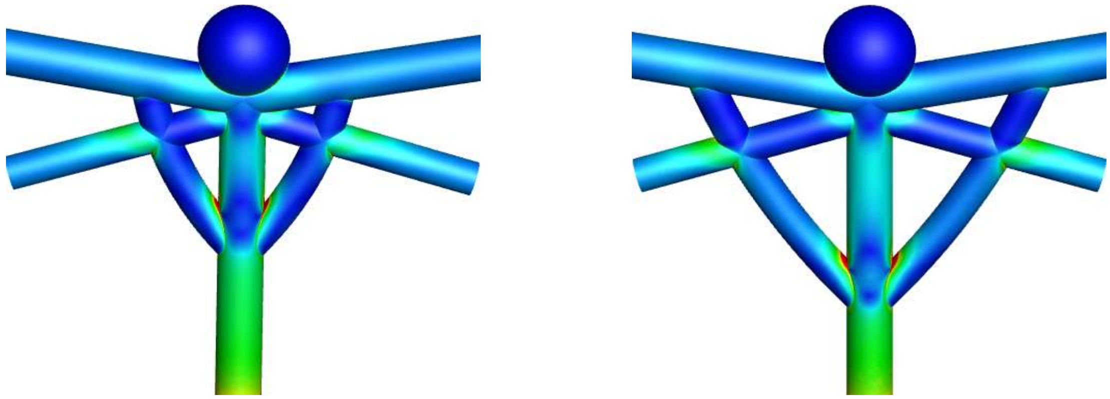

(c) (d)

Figure 11. Wall Shear Stress (WSS) contours at the apex of the systolic phase (0.145 s) for cases 1 to 4, as specified in Table 1.

Figure 11(a-d) depicts the wall shear stress (WSS) of the artery wall at the apex of the systolic phase across several geometric models. Figures 11(a) and 11(b) represent cases 1 and 2, while Figures 11(c) and 11(d) exemplify cases 3 and 4. The analysis of these scenarios reveals that the WSS markedly diminished in the aneurysm and the neighboring PCA and SCA regions as a result of the bypass graft. Conversely, extensive WSS is observed at the intersection of bypass arteries and the basilar artery. In cases 1, 2, and 4, the maximum wall shear stress (WSS) at the aneurysm wall decreased to roughly 6.49%, 27.32%, and 48.56%, respectively, however in case 3, WSS emerged by 0.47% compared to the model without bypass. Consequently, at the PCA artery wall, the maximum WSS decreased by approximately 15.15%, 32.88%, 20.85%, and 55.88%, respectively. Furthermore, at the SCA wall, the peak WSS was diminished by approximately 42.59%, 21.19%, 34.67%, and 36.75% for cases 1 through 4, respectively.

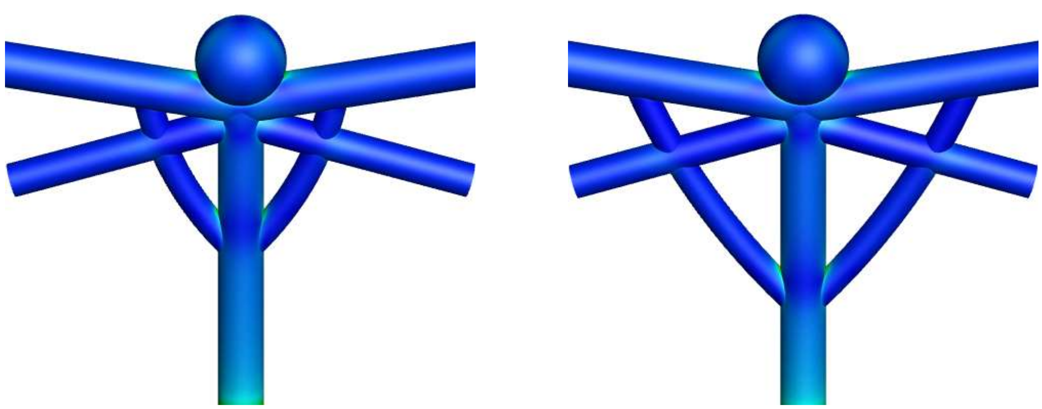

(a) (b)

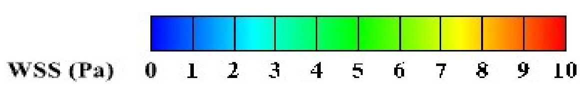

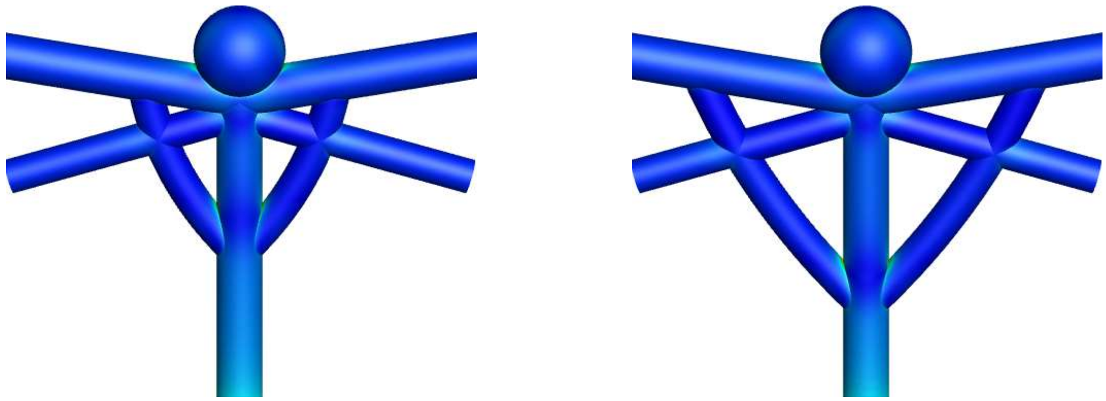

(c) (d)

Figure 12. Illustrations of Wall Shear Stress (WSS) at the end of the diastolic phase (0.8 s) for cases 1 to 4, as specified in Table 1.

The wall shear stress (WSS) of the arterial wall at the end of the diastolic phase is depicted in Figure 12(a-d), which illustrates the results of various geometric models. The first and second cases are depicted in Figures 12(a) and 12(b), respectively, while Cases 3 and 4 are illustrated in Figures 12(c) and 12(d). After doing an examination of these scenarios, it was discovered that the WSS had significantly decreased in the aneurysm as well as in the nearby PCA and SCA regions as a consequence of the bypass graft. On the other hand, substantial WSS is seen at the point where the basilar artery and the bypass arteries have reached their intersection. When compared to the model that did not include a bypass, the maximum wall shear stress (WSS) at the aneurysm wall dropped to approximately 25%, 26.85%, 11.24%, and 37.92%, respectively, in cases 1 through 4. Because of this, the maximum WSS fell by roughly 10.24%, 13.86%, 7.35%, and 25.54%, respectively, at the wall of the PCA artery. Furthermore, the peak WSS at the SCA wall was reduced by approximately 57.69%, 47.19%, 54.88%, and 59.08% for cases 1 through 4, respectively.

5. DISCUSSION

Early detection and treatment are crucial for cerebral aneurysms because of the high death rates associated with these diseases. These aneurysms can be treated surgically using a variety of techniques, including clipping, wrapping and clipping, coil embolization, high-porosity mesh (HPM) stents, and bypass procedures[24-31].Researchers, Feng et al. [34] showed that while other methods of fixing aneurysm neck avulsion failed, the clip-on-wrapping technique was effective. There are some restrictions regarding the location, size, and shape of the aneurysm that must be met in order for clipping to be an effective choice for ruptured aneurysms [25, 35]. The coiling operation is a common and significant alternative to other methods used to treat cerebral aneurysms. Nevertheless, coil displacement is a major risk factor for embolization treatments. In mild situations, it can cause infarcts that cause asymptomatic strokes; in extreme cases, it can block key branches and cause substantial damage to region [24]. Using an HPM stent can decrease blood flow velocity, pressure, wall shear stress, and energy loss within the aneurysm by 30-40%, according to Qiu et al. [25], who used the stent approach. The potential for problems such thrombosis, vascular injury, in-stent restenosis, stent displacement and migration, and other similar issues makes its usage questionable [24].In these circumstances, bypass procedures such extracranial-intracranial (EC-IC) or intracranial-

intracranial (IC-IC) are employed to address basilar tip aneurysms [24, 26, 35, 36]. In a study utilizing a model of an idealized basilar tip aneurysm, Kurşun et al. [26] investigated flow velocity, pressure, and wall shear stress (WSS), revealing that pressure and WSS can be reduced by 40-70% at the aneurysm wall through a bypass technique. Nonetheless, their model possesses certain limitations, which were stated in the introductory section, and the current study has addressed and rectified those shortcomings.

Nevertheless, this study utilized numerical methods to examine the impact of bypass vessel geometry and position of the bypass link on the aneurysm wall's pressure and shear stresses as well as the velocity within the aneurysm. Accordingly, utilizing clinical data particular to individual patients [37], this idealized basilar tip aneurysm model was developed. Despite structural differences between real and ideal basilar tip cerebral aneurysms, model validation revealed very similar shear stress values on the aneurysm wall.

6. CONCLUSION

The present study investigated the flow characteristics inside a three-dimensional computational model of basilar tip aneurysm with and without complete bypass graft. A transient, laminar, single phase fluid flow model was adopted for this study, and Finite Volume method was used to solve the governing equations. Key findings of pressure for the studied cases at the peak of the systolic phase that emerged from this computer simulation includes:

- For case 1, averaged pressure, averaged WSS reduced by26.139%, 35.179%at the aneurysm wall, and velocity magnitude reduced by 80.78% at the point P_1 in the aneurysm, while along the line EF, average velocity dropped to 22.467%.
- For case 2, average pressure, averaged WSS reduced by 30.448%, 46.457% at the aneurysm wall and velocity magnitude reduced by 85.85% at the point P_1 in the aneurysm. Also, average velocity reduced to 33.701% along the line EF.
- For case 3, averaged pressure, averaged WSS decreased to~33.332%, ~27.869% at the aneurysm wall, and velocity magnitude reduced by 36.76% at the point P_1 in the aneurysm. Also, averaged velocity decreased by 34.802% along with EF.
- For case 4, averaged pressure, averaged WSSreduced by 37.979%, 56.662% at the aneurysm wall, and velocity magnitude reduced by 92.91% at the point P_1 in the aneurysm. Also, along with EF, averaged velocity dropped to ~44.934%.
- The mass flow rate at the PCA outlet decreased by ~14.89%, ~32.36%, ~16.28%, and ~20.11% for cases 1 to 4 relative to the without-bypass model.
- Conversely, at the SCA outlet, the mass flow rate expanded by ~42.35%, ~91.88%, ~86.29%, and ~57.13% for the corresponding cases analyzed in this study.

By analyzing data, it appears that case 4 is an appropriate choice for bypass surgery, but it needs to be validated by an in vitro experiment. The current simulation utilizes an idealized aneurysm model; nonetheless, it is limited by the absence of patient-specific treatment outcomes, which will be addressed in future modeling explorations. In vitro and ex vivo experimental trials will be considered in further study plans to achieve successful simulation and experimental outcomes.

ACKNOWLEDGEMENT

All authors want to expose their thankfulness to each involvement for accomplishing this research work. This research received assistance from Ahsanullah University of Science and Technology, Dhaka, Bangladesh, under Project ID: AIRG/2024/A&S/06/17.

Credit authorship contribution statement

Nusrat Tamanna Mim: Data curation, Investigation, Methodology, Software, Validation, Writing-original draft; **Sorowar Hossain:** Formal analysis, Resources, Visualization, Software, Validation, Writing-original draft; **Muhammad Sajjad Hossain:** Conceptualization, Investigation, Formal analysis, Project administration, Methodology, Visualization, Funding, Supervision, writing original draft, writing review and editing.

Funding

This research paper has no external funding.

Declaration of interest

Regarding the research, writing, and/or publication of this article; the author(s) state that they have no potential conflicts of interest.

Data availability

No data was used for the research described in the article.

REFERENCES

[1] N. Chalouhi, B. L. Hoh, and D. Hasan, "Review of cerebral aneurysm formation, growth, and rupture," Stroke, vol. 44, no. 12, pp. 3613-3622, 2013.

[2] J. L. Brisman, J. K. Song, and D. W. Newell, "Cerebral aneurysms," New England journal of medicine, vol. 355, no. 9, pp. 928-939, 2006.

[3] M. H. Vlak, A. Algra, R. Brandenburg, and G. J. Rinkel, "Prevalence of unruptured intracranial aneurysms, with emphasis on sex, age, comorbidity, country, and time period: a systematic review and meta-analysis," The Lancet Neurology, vol. 10, no. 7, pp. 626-636, 2011.

[4] "Brain aneurysm statistics and facts." Brain Aneurysm Foundation. https://www.bafound.org/statistics-and-facts/ (accessed March 13, 2025).

[5] E. S. Connolly Jr et al., "Guidelines for the management of aneurysmal subarachnoid hemorrhage: a guideline for healthcare professionals from the American Heart Association/American Stroke Association," Stroke, vol. 43, no. 6, pp. 1711-1737, 2012.

[6] J.-h. DAI, G.-h. DING, and J.-q. GONG, "Hemodynamic 2-D numerical simulation of an intracranial aneurysm [J]," Journal of Fudan University (Natural Science), vol. 43, no. 3, pp. 392-396, 2004.

[7] Y. Hoi, S. H. Woodward, M. Kim, D. B. Taulbee, and H. Meng, "Validation of CFD simulations of cerebral aneurysms with implication of geometric variations," 2006.

[8] M. D. Ford et al., "PIV-measured versus CFD-predicted flow dynamics in anatomically realistic cerebral aneurysm models," 2008.

[9] E. Boutsianis et al., "CFD and PTV steady flow investigation in an anatomically accurate abdominal aortic aneurysm," 2009.

[10] P. M. Munarriz, P. A. Gómez, I. Paredes, A. M. Castaño-Leon, S. Cepeda, and A. Lagares, "Basic principles of hemodynamics and cerebral aneurysms," World neurosurgery, vol. 88, pp. 311-319, 2016.

[11] J.-w. Zhao, W.-y. Yin, G.-h. Ding, X.-j. Yang, W.-c. Shi, and X.-l. Zhang, "Numerical simulation and analysis on the hemodynamics of an elastic aneurysm," Journal of Hydrodynamics, vol. 20, no. 2, pp. 216-224, 2008.

[12] J. Bernsdorf and D. Wang, "Non-Newtonian blood flow simulation in cerebral aneurysms," Computers & Mathematics with Applications, vol. 58, no. 5, pp. 1024-1029, 2009.

[13] R. Razaghi, H. Biglari, and A. Karimi, "Risk of rupture of the cerebral aneurysm in relation to traumatic brain injury using a patient-specific fluid-structure interaction model," Computer Methods and Programs in Biomedicine, vol. 176, pp. 9-16, 2019.

[14] L. Sun, J. Wang, M. Li, M. Li, and Y. Zhu, "The contribution of wall shear stress insult to the growth of small unruptured cerebral aneurysms in longitudinal 3D-TOF-MRA," Journal of the Neurological Sciences, vol. 413, p. 116798, 2020.

[15] M. A. A. Sheikh, A. S. Shuib, and M. H. H. Mohyi, "A review of hemodynamic parameters in cerebral aneurysm," Interdisciplinary Neurosurgery, vol. 22, p. 100716, 2020.

[16] H. Kimura et al., "Newly identified hemodynamic parameter to predict thin-walled regions of unruptured cerebral aneurysms using computational fluid dynamics analysis," World Neurosurgery, vol. 152, pp. e377-e386, 2021.

[17] S. Fujimura et al., "Computational fluid dynamic analysis of the initiation of cerebral aneurysms," Journal of neurosurgery, vol. 137, no. 2, pp. 335-343, 2021.

[18] A. G. Rahma and T. Abdelhamid, "Hemodynamic and fluid flow analysis of a cerebral aneurysm: a CFD simulation," SN Applied Sciences, vol. 5, no. 2, p. 62, 2023.

[19] G. Singh, P. N. Yadav, S. Gupta, and A. Chanda, "Biomechanical modeling of aneurysm in posterior cerebral artery and posterior communicating artery: Progression and rupture risk," Brain Multiphysics, vol. 4, p. 100069, 2023.

[20] G. Singh, P. N. Yadav, S. Gupta, and A. Chanda, "Modeling of aneurysm progression in anterior cerebral arteries to estimate rupture risk: A computational study," Biomedical Engineering Advances, vol. 6, p. 100106, 2023.

[21] N. Kaneko, T. Mashiko, K. Namba, S. Tateshima, E. Watanabe, and K. Kawai, "A patient-specific intracranial aneurysm model with endothelial lining: a novel in vitro approach to bridge the gap between biology and flow dynamics," Journal of NeuroInterventional Surgery, vol. 10, no. 3, pp. 306-309, 2018.

[22] P. Jiang et al., "Hemodynamic characteristics associated with thinner regions of intracranial aneurysm wall," Journal of Clinical Neuroscience, vol. 67, pp. 185-190, 2019.

[23] S.-Q. Hu, R.-D. Chen, W.-D. Xu, and J.-S. Yu, "Risk factors for the rupture of mirror middle cerebral artery aneurysm using computer-assisted semiautomated measurement and hemodynamic analysis," Journal of Stroke and Cerebrovascular Diseases, vol. 31, no. 12, p. 106841, 2022.

[24] J. Zhao, H. Lin, R. Summers, M. Yang, B. G. Cousins, and J. Tsui, "Current treatment strategies for intracranial aneurysms: an overview," Angiology, vol. 69, no. 1, pp. 17-30, 2018.

[25] X.-n. Qiu, Z.-m. Fei, J. Zhang, and Z.-m. Cao, "Influence of high-porosity mesh stent on hemodynamics of intracranial aneurysm: A computational study," Journal of Hydrodynamics, vol. 25, no. 6, pp. 848-855, 2013.

[26] B. Kurşun, L. Uğur, and G. Keskin, "Hemodynamic effect of bypass geometry on intracranial aneurysm: a numerical investigation," Computer methods and programs in biomedicine, vol. 158, pp. 31-40, 2018.

[27] B. Bisighini, M. Aguirre, B. Pierrat, and S. Avril, "Patient-specific computational modelling of endovascular treatment for intracranial aneurysms," Brain Multiphysics, vol. 5, p. 100079, 2023.

[28] P. Nair et al., "Hemodynamic characterization of geometric cerebral aneurysm templates treated with embolic coils," Journal of biomechanical engineering, vol. 138, no. 2, p. 021011, 2016.

[29] S.-i. Sugiyama et al., "Blood flow into basilar tip aneurysms: a predictor for recanalization after coil embolization," Stroke, vol. 47, no. 10, pp. 2541-2547, 2016.

[30] T. Ishii et al., "Hemodynamic and morphologic factors related to coil compaction in basilar artery tip aneurysms," World Neurosurgery, vol. 155, pp. e95-e110, 2021.

[31] Z.-H. Jin, M. B. Gerdroodbary, P. Valipour, M. Faraji, and N. H. Abu-Hamdeh, "CFD investigations of the blood hemodynamic inside internal cerebral aneurysm (ICA) in the existence of coiling embolism," Alexandria Engineering Journal, vol. 66, pp. 797-809, 2023.

[32] L. Peng, J. Chen, Y. Cheng, N. Lv, H. Gao, and B. Bai, "The hemodynamic effect of flow diverter treatment of intracranial bifurcation aneurysms," Journal of Medical and Biological Engineering, vol. 40, pp. 851-857, 2020.

[33] Y. Boite, T. Suaiden Klein, R. de Andrade Medronho, and E. Wajnberg, "Numerical simulation of flow-diverting stent: comparison between branches in bifurcation brain aneurysm," Biomechanics and Modeling in Mechanobiology, vol. 22, no. 6, pp. 1801-1814, 2023.

[34] Y.-g. Feng et al., "Clip-on-wrapping with dura mater to treat intracranial aneurysm neck avulsion: Case reports and review of the literature," Clinical Neurology and Neurosurgery, vol. 115, no. 10, pp. 2284-2287, 2013/10/01/ 2013.

[35] B. A. Strickland, F. Attenello, and J. J. Russin, "Extracranial to intracranial bypass for the treatment of cerebral aneurysms in the pediatric population," Journal of Clinical Neuroscience, vol. 34, pp. 6-10, 2016/12/01/ 2016.

[36] A. Quiñones-Hinojosa, R. Du, and M. T. Lawton, "Revascularization with saphenous vein bypasses for complex intracranial aneurysms," Skull Base, vol. 15, no. 02, pp. 119-132, 2005.

[37] S. Appanaboyina, F. Mut, R. Löhner, C. Putman, and J. Cebral, "Simulation of intracranial aneurysm stenting: techniques and challenges," Computer Methods in Applied Mechanics and Engineering, vol. 198, no. 45-46, pp. 3567-3582, 2009.

[38] V. Kashyap, B. Arora, and S. Bhattacharjee, "A computational study of branch-wise curvature in idealized coronary artery bifurcations," Applications in Engineering Science, vol. 4, p. 100027, 2020.